

# Submillimetre sources in rich cluster fields – source counts, redshift estimates, and cooling flow limits

Scott C. Chapman,<sup>1</sup> Douglas Scott,<sup>2</sup> Colin Borys,<sup>2</sup> and Gregory G. Fahlman<sup>2,3</sup>

<sup>1</sup>Observatories of the Carnegie Institution of Washington, Pasadena, CA 91101, U.S.A.

<sup>2</sup>University of British Columbia, Department of Physics & Astronomy, Vancouver BC V6T 1Z4, Canada

<sup>3</sup>Canada-France-Hawaii Telescope, Kamuela, Hawaii 96743, USA

Accepted ... ; Received ... ; in original form ...

## ABSTRACT

Recent submillimetre surveys have revealed a population of dusty, high redshift sources of great cosmological significance for understanding dust-enshrouded star formation in distant galaxies, and for determining the origin of the far-IR background. In this paper, we analyze nine rich cluster fields mapped at 850  $\mu$ m and 450  $\mu$ m with the SCUBA array on the James Clerk Maxwell telescope. Lensing models of the clusters are developed in order to derive accurate source counts for our sample. VLA maps of the same clusters are used to help constrain the redshift distribution of our SCUBA detections. Implications for high redshift galaxies and for the far-IR background are discussed. We also provide limits on distributed dust produced by cooling flows in these clusters.

**Key words:** Infrared: galaxies – Submillimetre – galaxies: formation – galaxies: evolution

## 1 INTRODUCTION

The submillimetre waveband has recently become an invaluable tool for investigating the properties of high redshift galaxies. An early result using the Sub-millimetre Common User Bolometer Array (SCUBA – Holland et al. 1999) by Smail, Ivison and Blain (1997) showed that a much larger population of dusty, high redshift galaxies existed than previously thought. The existence of these dusty, sub-mm galaxies at relatively high redshifts have now been confirmed in several surveys (Hughes et al. 1998; Barger et al. 1998, 1999a; Eales et al. 1999; Lilly et al. 1999a; Blain et al. 1999). Such sub-mm sources could be of great cosmological significance – they may comprise a substantial fraction of the Far-Infrared Background (FIRB – Puget et al. 1996, Hauser et al. 1998, Lagache et al. 1999). Additionally, they could be an important source of CMB anisotropy at arcsecond scales (Scott & White 1999), and certainly the dominant source of sky fluctuations at  $\sim 1$ mm, at least out of the galactic plane (Hughes et al. 1998, Borys, Chapman & Scott 1999). Our understanding of the star-formation history of galaxies depends critically on the properties of these sub-mm sources: this population is responsible for a substantial fraction of the total star formation output in the early Universe and holds important information about how galaxies formed and evolved (e.g. Blain & Longair 1993, Guiderdoni et al. 1997, Blain et al. 1998). They appear to be the high redshift counterparts of well-studied nearby ultra-luminous

IR galaxies (Sanders & Mirabel 1996), and can be plausibly interpreted as the formation sites of galactic spheroids through mergers of gaseous disk systems (e.g. Sanders 1999, Lilly et al. 1999a).

Much work has gone into identifying just what types of galaxies make up this sub-mm bright population, and what mechanisms may be responsible for their rest-frame far-IR emission (Smail et al. 1998; Hughes et al. 1998; Ivison et al. 1998b; Lilly et al. 1999b; Frayer et al. 1998; Frayer et al. 1999; Frayer et al. 2000; Chapman et al. 1999; Ivison et al. 2000; Chapman et al. 2000; Bertoldi et al. 2000; Gear et al. 2000). However, the numbers of sub-mm source detections are still relatively small. In an effort to increase the statistics and broaden the source count baseline, we have undertaken a sub-mm survey including both blank sky (Borys et al. in preparation) and cluster fields. Our cluster sample is complementary to that of Smail, Ivison, and Blain (1997, 1998) who pioneered this approach using SCUBA on the JCMT. These cluster fields benefit from the lensing by the foreground cluster mass at  $z < 1$ , enhancing sensitivity to the dusty galaxies at higher redshifts.

Our cluster sample consists of nine clusters at redshifts 0.2–0.8, originally selected to search for both distributed cool dust (cooling flows – see Edge et al. 1999) and the Sunyaev-Zel'dovich (SZ) effect (Birkinshaw 1999; Andreani et al. 1999). Although we found no convincing evidence for distributed emission, our SCUBA maps have revealed significant source detections, as expected from the counts from

other surveys (e.g. Blain et al. 1999, Barger et al. 1999b). This further demonstrates that sub-mm surveys provide an efficient means of identifying a population of dusty AGN and/or star-forming galaxies, possibly at very high redshifts. In addition, a few weak sources appear coincident with radio-bright central galaxies in the clusters, possibly associated with the strong cooling flows suggested by the x-ray profiles. In this paper, we describe possible sources found in the cluster fields, and present the resulting source counts. Existing VLA maps are used to place limits on the redshift distribution of the sample. We conclude by discussing the implications for high redshift galaxies and the FIRB.

## 2 OBSERVATIONS

### 2.1 JCMT data

Nine clusters were observed with the SCUBA instrument on the James Clerk Maxwell Telescope, resulting in 17 significant source detections greater than  $3\sigma$ . During 4 observing runs throughout 1998 and 1999, we operated the 91 element Short-wave array at  $450\mu\text{m}$ , and the 37 element Long-wave array at  $850\mu\text{m}$  simultaneously, in JIGGLE mode, and additionally the single photometry pixel at  $1350\mu\text{m}$  for some sources, giving half-power beam widths of 7.5, 14.7, and 21.0 arcsec respectively. Additionally,  $850/450\mu\text{m}$  PHOTOMETRY mode followup on 3 of the sources was performed, confirming their existence and flux densities. The central pixel of SCUBA was fixed on the source, as defined by the centroid of the *ROSAT* imaging (Crawford et al. 1999). For mapping, the standard 64-point jiggle pattern was employed to fully sample the  $450$  and  $850\mu\text{m}$  arrays. The effective integration times (time spent on and off source derived from the number of 64 point integrations obtained, which excludes overheads) are presented in Table 1 for each cluster. For  $1350\mu\text{m}$  photometry we used the 9-point jiggle pattern to reduce the impact of pointing errors by averaging the source signal over a slightly larger area than the beam, resulting in greater photometric accuracy. Whilst jiggling, the secondary was chopped at 7.8125 Hz with chop throws between 40 and 120 arcsec in azimuth, with smaller throws used under worse atmospheric conditions or when the projected core radius for a cluster was smaller.

Pointing was checked hourly on blazars and a sky-dip was performed to measure the atmospheric opacity directly. The RMS pointing errors were below 2 arcsec, while the average atmospheric zenith opacities at  $450\mu\text{m}$ ,  $850\mu\text{m}$  and  $1350\mu\text{m}$  were fairly stable and generally quite good with  $\tau_{850}$  ranging from 0.15 to 0.36. Some short time-scale variations, presumably due to the atmosphere, caused some parts of the data-set to be noisier, and these noisiest sections were excluded.

The data were reduced using the Starlink package SURF (Scuba User Reduction Facility, Jenness et al. 1998). Spikes were first carefully rejected from the data, followed by correction for atmospheric opacity and sky subtraction using the median of all the array pixels, except for obviously bad pixels (the  $1350\mu\text{m}$  pixel currently has no provision for subtracting sky variations using the other wavelength pixels). We then weighted each pixel by its timestream inverse variance, relative to the central pixel. Multiple scans on the

same cluster field, and sky rotation, ensure that (in most cases) each point of the map is covered by many bolometers. Even with the inverse variance weighting, excessively bad pixels still appeared to degrade the map, and were therefore clipped from the data prior to rebinning into the final maps. The data were then calibrated against standard planetary or compact H $\text{II}$  region sources, observed during the same nights as the clusters. Uncertainties at  $850\mu\text{m}$  and  $1350\mu\text{m}$  are estimated to be around 10 per cent, while at  $450\mu\text{m}$  they could be as high as 25 per cent. Note that calibration uncertainties do not affect the S/N level for our detections, only the overall flux densities reported.

### 2.2 Archive VLA data

VLA maps at 4.9 GHz in the C configuration were obtained for five clusters in our sample courtesy of A. Edge. The effective resolution in the images is 5 arcsec. More details of the reduction and analysis of similar maps are given in Edge et al. (1999a). Typical  $1\sigma$  sensitivities lie around  $60\mu\text{Jy}$ . In addition, an archive 1.4 GHz map for Abell 2219 was obtained courtesy of F. Owen, reaching a  $1\sigma$  limit of  $\sim 39\mu\text{Jy}$  per 2 arcsec beam.

For the remaining clusters, VLA data presented in Stocke et al. (1999) at 1.4 GHz in the B configuration, was used to set limits and identify counterpart positions. Typical 1.4 GHz sensitivities in these maps are  $65\mu\text{Jy}$  RMS.

## 3 SOURCE CATALOGUE

The  $850\mu\text{m}$  SCUBA maps for the clusters showing significant source detections are presented in Figs. 1 and 2. Any real objects in our maps are expected to be unresolved and will typically appear as a positive point spread function with  $\text{FWHM} \sim 15$  arcsecs at  $850\mu\text{m}$ . For most of our maps, we do not expect to see negative signatures for our sources, as the individual scans coadded in the map have different chop throws and directions, diluting the effect of off-beams. We also chopped out of the field in most cases. The edges of the maps incur a rapid rise in noise level due to incomplete sampling of the sky for the outer bolometers of the SCUBA array. Eales et al. (1999) simulated the incomplete sampling at the field edge and found that any spurious sources in Monte Carlo simulations tended to appear in this region. We have therefore clipped the 14 arcsec edge regions in our maps where the noise level increases by a factor  $\gtrsim 2$  times that at the field center.

As the signal-to-noise ratio (S/N) is low for individual pixels, we use a template fitting method for source detection to achieve a maximum gain in S/N, similar to that used in Eales et al. (1999). The cluster maps are convolved with the beam map obtained by imaging Mars, and all peaks greater than  $3\sigma$  are extracted as potential sources. We checked the convolved maps carefully against the raw data to ensure that no residual bad pixels were identified as sources. We also note that there are no strong negative sources in our maps.

Sensitivity limits for deep SCUBA integrations have now been fairly well characterized (Smail et al. 1997, Hughes et al. 1998, Eales et al. 1998, Barger et al. 1999b). But at these low S/N levels, we must be careful to consider possible

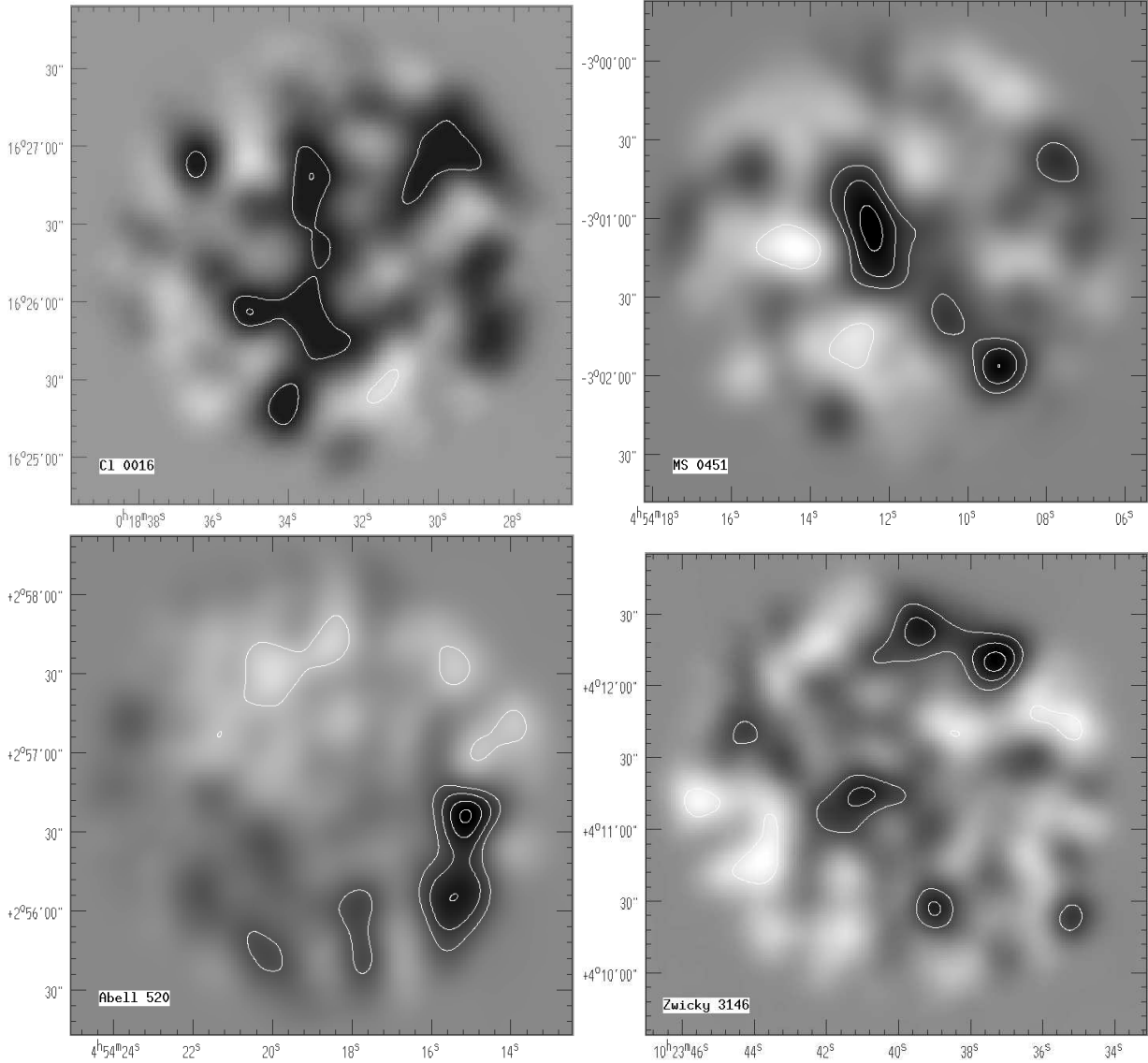


**Figure 1.** Cluster field images at  $850\mu\text{m}$ , convolved with the SCUBA 14.7 arcsec beam. Dark shading is positive flux density, while lighter shading is negative. All contour levels indicate the number of sigma above the background noise estimated from the central regions of the beam-convolved images, starting at  $2\sigma$ , with intervals of  $1\sigma$ . These noise levels correspond approximately to the tabulated values (Tables 1&2), which were derived from the raw data. Top row: Cl0016+16 (left); MS 0451-03 (right). Bottom row: Abell 520 (left); Zwicky 3146 (right).

systematic noise effects. There are currently five identified components which contribute to the overall SCUBA noise level: (i) photon noise from the sky; (ii) telescope and instrumental noise; (iii) blanked-off detector Johnson, phonon and amplifier noise; (iv) excess photon noise from the optics; (v) excess radiative load in the dewar. The noise terms add in quadrature, and the estimate for the relative contributions at the average sky emissivity for our survey ( $\langle\tau_{850}\rangle \simeq 0.2$ ) are respectively 29, 25, 17, 13, and 16 per cent (W. Holland private communication). Thus sky noise is the largest source, but does not dominate the others. Nevertheless, we expect the noise to integrate down with time. This will not be true of one additional source of noise: ‘confusion noise’ arising from fluctuations due to undetected sources. However, the level is essentially negligible for these observations

- Blain et al. (1998) quote a value of  $\sigma_{\text{conf}} = 0.44\text{ mJy}$ , derived from their source counts, while we find that any reasonable extrapolation of the counts (together with the constraint of not over-producing the FIRB) leads to a variance of no more than 0.5 mJy. We can therefore safely ignore confusion noise. However, it is worth pointing out that lensing by the clusters effectively allows us to probe below the confusion limit of say  $3\sigma_{\text{conf}}$ .

With transient noise and bad pixels from scan to scan, our confidence in many of the detections is reinforced by dividing the data into two parts and seeing evidence of the sources (at the  $> 2\sigma$  level) appear in both. Multi-wavelength detections also substantially strengthen our confidence in a source. Although the  $450\mu\text{m}$  channel is typically not sensitive enough to detect these objects, especially those lying at

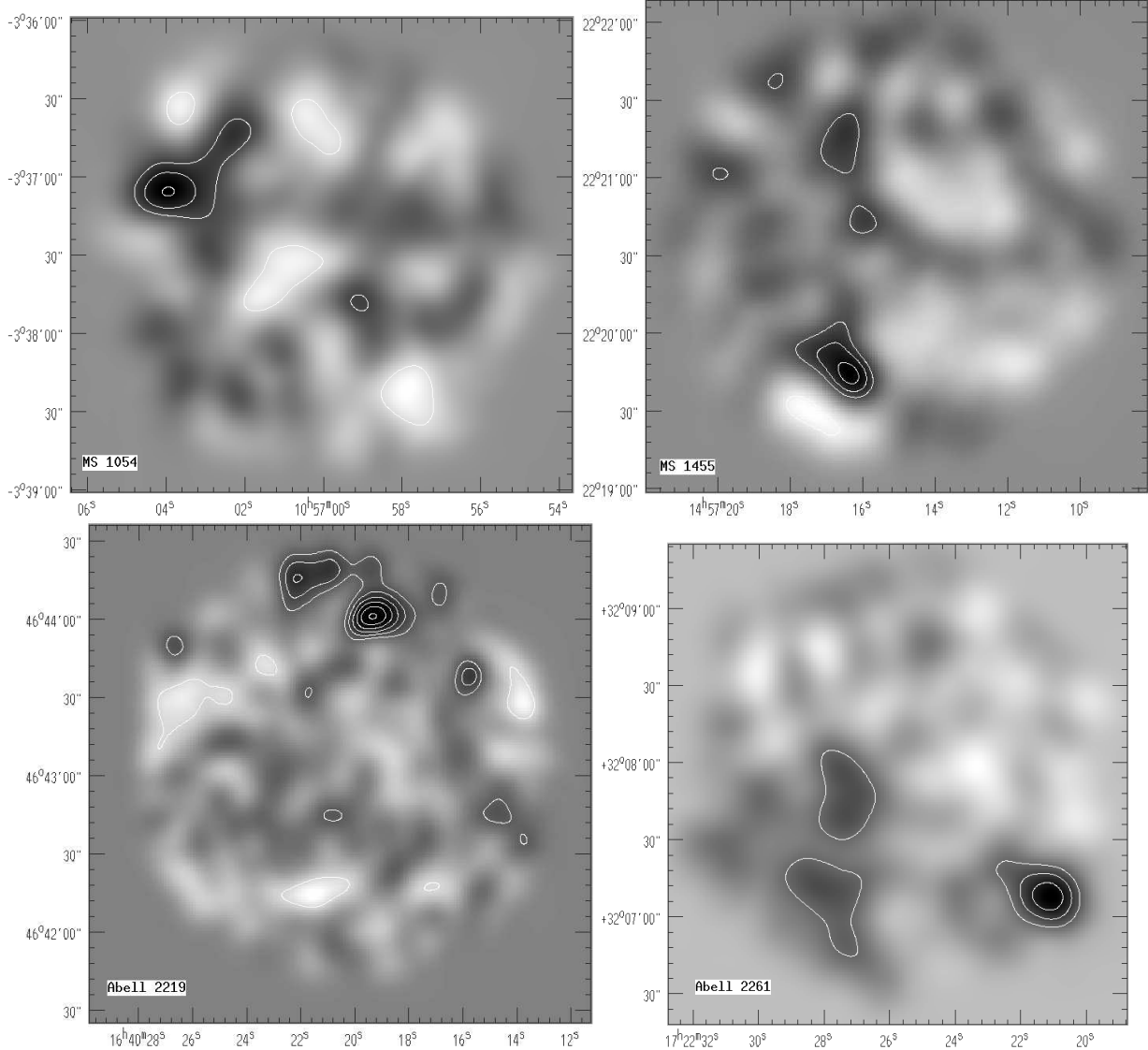


**Figure 2.** SCUBA maps at  $850\mu\text{m}$  continued. Contours are the same as Fig. 1. Top row: MS 1054-03 (left); MS 1455+22 (right). Bottom row: Abell 2219 (left); Abell 2261 (right).

higher redshifts, many more of them may be observable at  $1350\mu\text{m}$  with deeper photometry than we have currently obtained. Three sources have been subsequently verified through PHOTOMETRY followup observations (MS 0451-A, Abell 2261-A, and MS 1455-A). These are discussed in the individual source section (4.2).

Empirically, the localized noise levels are seen to integrate down in our maps roughly as  $t^{-1/2}$  (see also Ivison et al. 1998a). We note that in a typical  $850\mu\text{m}$  SCUBA field of 5.2 square arcmin with  $\sim 100$  independent beams we expect only  $\sim 0.1$  spurious  $3\sigma$  peaks from Gaussian noise, and  $\ll 1$  spurious  $4\sigma$  peak from our whole survey.

The completeness of a set of detections has typically been established using synthetic source recovery techniques in Monte Carlo simulations (Smail et al. 1997, Hughes et al. 1998). Our  $3\sigma$  and source catalogues corresponds approximately to the 80 per cent completeness level found in Smail

et al. (1997). We estimate that our  $4\sigma$  catalogue is more than 90 per cent complete.

Our sub-mm observations of the clusters are presented in Tables 1 and 2. Table 1 lists the clusters, coordinates, and redshifts, along with total exposure time (based on the number of integrations). The last four columns present the average  $850\mu\text{m}$  and  $450\mu\text{m}$  sensitivities achieved after subtracting sources  $> 3\sigma$  from the field, and the number of sources detected at greater than the  $3\sigma$  and  $4\sigma$  levels. Table 2 lists the properties of the detected sources, with coordinates and observed flux densities in each of the three sub-mm wavelength bands. These sub-mm detections and upper limits (upper limits are given as 95 per cent Bayesian confidence regions, assuming Gaussian errors and neglecting the negative flux region) at  $1350$ ,  $850$ , and  $450\mu\text{m}$  provide rough photometric estimates of the source redshifts (see e.g. Hughes et al. 1998). However, the addition of radio data significantly increases confidence in these photometric redshifts. The final

two columns list the VLA radio flux limits, and estimates of the redshift from the sub-mm and radio data, as described below.

## 4 PROPERTIES OF INDIVIDUAL SOURCES

### 4.1 VLA radio counterparts

Radio counterparts to sub-mm sources are expected due to the synchrotron emission resulting from either an AGN or shocked gas in supernovae remnants from a starburst (e.g. Richards et al. 1999). Given the small number density of radio emitting objects, the chances of finding a 1.4 GHz VLA object of  $> 200 \mu\text{Jy}$  in our error circle by chance is much less than 1 per cent (Richards et al. 1998). By contrast, identifying optical counterparts to the SCUBA-selected galaxies is a non-trivial matter for two main reasons: 1) the beam-size at  $850 \mu\text{m}$  (the optimal wavelength for these studies) is  $\sim 15$  arcsec, with pointing errors for the telescope of order 2 arcsec; 2) the large, negative K-corrections (i.e. increase in flux density as the objects are redshifted) of dusty star-forming galaxies at these wavelengths imply that sub-mm observations can detect such objects at  $z > 1$  in an almost distance-independent manner. Thus several candidate optical galaxies are often present within the uncertainty of the sub-mm detection, along with the possibility that the actual counterpart is at much higher redshift and undetectable with current optical imaging. In this paper we restrict our attention to radio counterparts, and defer detailed optical analysis of the sub-mm source positions to a separate paper.

Carilli & Yun (1999, 2000 – CY) recently demonstrated that crude redshift estimates for distant dusty galaxies could be obtained in the absence of an optical counterpart using the spectral index between the sub-mm ( $850 \mu\text{m}$ ) and radio (1.4 GHz) wavebands ( $\alpha_{1.4}^{850}$ ), with a mean galaxy model parameterized as  $z = 0.050 - 0.308\alpha + 12.4\alpha^2 - 23.0\alpha^3 + 14.9\alpha^4$ . The model SEDs used by CY are based largely on lower redshift observations, however they are able to successfully describe the few high-redshift galaxies which have multi-wavelength radio and sub-mm observations available. Follow up studies by Blain (1999) have shown that if lower dust temperatures are adopted for the sub-mm population than are seen in the local sources used in CY's models, then the allowed redshifts are slightly lower for a given value of  $\alpha_{1.4}^{850}$ . The isolated cases which do not fall within the CY model predictions are known to have strong radio-loud AGN components. The important point is that the derived redshift provides a robust lower limit, irrespective of the nature of the emission mechanism, AGN or starburst, since an AGN contribution to the radio emission flattens the radio spectrum. The modest scatter between the models in CY suggests that the  $\alpha_{1.4}^{850}$  technique currently provides the most useful limit on the redshifts of sub-mm galaxies, in the absence of an optical counterpart.

Smail et al. (2000) recently applied the CY analysis to deep radio observations of the complete sample of SCUBA-selected galaxies from their cluster lens survey (Smail et al. 1998, Ivison et al. 2000), revealing a higher redshift distribution than previously expected from optical follow-up work. Using existing VLA data for our SCUBA cluster sample, we can thus constrain the redshift distribution of our

population and set the stage for optical/near-IR follow-up identifications.

We searched for radio counterparts around the nominal positions of the sub-mm sources based on the SCUBA astrometry. Positional errors for SCUBA sources from the literature which were clearly identified in radio and optical wavelengths (e.g. Ivison et al. 1998b, Frayer et al. 1999) were  $\sim 6$  arcsec for  $4\sigma$  detections and  $\sim 8$  arcsec for  $3\sigma$  detections, and we use similar error circles for our analysis. Radio limits at 1.4 GHz for sources in A 520, Zw 3146, MS 1455, and A 2261, have been extrapolated from the value at 4.9 GHz, using a spectral index  $\alpha = 0.8$  (i.e.  $S \propto \nu^{-0.8}$ ) appropriate for star formation driven synchrotron emission. This provides a reasonable estimate of the source redshift using the CY relation (since a brighter radio counterpart leads to a lower redshift estimate, while an AGN component would flatten the spectrum giving rise to a higher redshift). The 1.4 GHz VLA data from Stocke et al. (1999) are used to derive limits for Cl 0016, MS 0451, and MS 1054, and an archive 1.4 GHz map of A 2219 (courtesy of F. Owen) was used to measure fluxes directly. In 5 cases, there were radio sources  $> 3\sigma$  lying within the error circle of the sub-mm beam. One of these may be a central cluster galaxy and is also discussed in the following section. The 15 arcsec by 15 arcsec region surrounding the sub-mm sources are shown in Fig. 3, with the apparent radio flux densities or limits listed in Table 2.

We use the CY relation (which is consistent with dust temperature  $T_d = 50 \text{ K}$ ) to generate these lower limits to the source redshifts. We note that the actual dust temperature in the sub-mm sources may be lower, bringing down the redshifts, or of course higher, thereby raising the inferred redshift. In general the constrained quantity is  $T_d/(1+z)$ .

### 4.2 Source characteristics and evidence for cluster members

We now discuss each cluster field in detail:

#### Cl 0016+16

The data for this cluster show a general positive excess at the  $\sim 2\sigma$  level, with 2 peaks barely reaching the  $3\sigma$  level in the convolved map (sources A and B). There are no 1.4 GHz VLA counterparts down to the  $200 \mu\text{Jy}$  level, although the bright  $2.7 \text{ mJy}$  radio source from Stocke et al. (1999) lies on a clear sub-mm peak which reaches  $2.6\sigma$  significance in the convolved map. The generally positive excess could be caused by a Sunyaev-Zel'dovich increment (core radius  $\sim 2$  arcmin – Carlstrom et al. 1999), which is too noisy in this map to detect with any confidence. However it may have some effect on the detectability of other sources in this field.

#### MS 0451–03

An unresolved source (B: SMMJ 04542–0301) is found to the West in this cluster, and there is north-south extended positive sub-mm emission over the x-ray centroid region, reaching  $4\sigma$  in the convolved map (A: SMMJ 04541–0302). An additional  $850 \mu\text{m}$  photometry observation centered on the elongated source reveals a detection of  $10.1 \pm 3.0 \text{ mJy}$ , which is consistent with the peak flux densities found along the source as well as the positional accuracy of the SCUBA map. This central source is offset by 20 arcsecs to the east from the brightest cluster galaxy (BCG), and 20 arcsecs to the west from a  $1.8 \text{ mJy}$  VLA source (Stocke et al. 1999). This detection could possibly represent cool dust associated

Table 1  
Sub-mm observations for the clusters in our sample

Cluster	R.A. <sup>a</sup> (J2000)	Dec. <sup>a</sup> (J2000)	$z$	Exposure time (ks)	$S_{850}^b(1\sigma)$ (mJy)	$S_{450}^b(1\sigma)$ (mJy)	$N(S_{850} > S_{\text{lim}})$	
							$3\sigma$	$4\sigma$
Cl 0016+16	00 18 33.2	+16 26 18	0.541	20.5	3.1	36	2	0
MS 0451-03	04 54 13.4	-03 01 47	0.550	14.1	4.2	181	2	2
Abell 520	04 54 19.0	+02 56 49	0.203	7.7	5.0	66	2	1
Zwicky 3146	10 23 39.6	+04 11 10	0.291	12.8	2.6	25	4	1
MS 1054-03	10 57 00.2	-03 37 27	0.833	7.7	4.3	103	1	0
MS 1455+22	14 57 15.1	+22 20 35	0.259	15.4	2.1	22	1	1
Abell 2163	16 15 34.1	-06 07 26	0.201	7.7	5.8	44	0	0
Abell 2219	16 40 20.5	+46 42 59	0.228	15.4	1.7	8	4	1
Abell 2261	17 22 24.1	+32 07 45	0.224	7.7	3.8	105	1	1
<b>Total</b>						<b>17</b>	<b>7</b>	

<sup>a</sup> x-ray centre – ROSAT archive.

<sup>b</sup> Measured RMS over the central 60 arcsec of the field after subtracting a scaled SCUBA beam profile from any identified sources in the region.

Table 2

Details of individual sources

Source		$S_{1350\mu m}^b$ (mJy)	$S_{850\mu m}^b$ (mJy)	$S_{450\mu m}^b$ (mJy)	$S_{1.4 \text{ GHz}}^c$ (mJy)	$z_{\text{est}}^d$ ( $\mu$ Jy)
Cl 0016						
A SMMJ 00186+1626		$9.9 \pm 3.3$	$7 \pm 34$	$<200$	$>1.8$	
B SMMJ 00186+1625		$9.8 \pm 3.2$	$-4 \pm 36$	$<200$	$>1.8$	
MS 0451						
A SMMJ 04541-0302		$16.8 \pm 4.2$	$24 \pm 181$	$<200$	$>2.2$	
B SMMJ 04542-0301 <sup>g</sup>		$19.1 \pm 4.2$	$-61 \pm 177$	$<200$	$>2.3$	
Abell 520:						
A SMMJ 04543+0257		$33.0 \pm 5.0$	$-39 \pm 67$	$<420$	$>2.2$	
B SMMJ 04543+0256		$16.2 \pm 5.1$	$13 \pm 70$	$<410$	$>1.6$	
Zwicky 3146						
A SMMJ 10237+0411	$1.7 \pm 3.9$	$9.3 \pm 2.5$	$15 \pm 23$	$482/2722^e$	$1.1(0.3)^e$	
B SMMJ 10237+0410		$9.2 \pm 2.5$	$-2 \pm 25$	543	1.1	
C SMMJ 10237+0412		$9.4 \pm 2.6$	$6 \pm 27$	$<450$	$>1.2$	
D SMMJ 10236+0412		$11.2 \pm 2.6$	$23 \pm 27$	467	1.3	
MS 1054						
A SMMJ 10571-0337	$15.2 \pm 5.4$	$14.8 \pm 4.3$	$12 \pm 103$	$<200/1600$	$2.1(0.8)$	
MS 1455:						
A SMMJ 14573+2220 <sup>g</sup>		$10.1 \pm 2.2$	$5 \pm 22$	$<294$	$>1.5$	
Abell 2219						
A SMMJ 16403+46440	$4.3 \pm 2.0$	$10.6 \pm 1.7$	$34 \pm 11$	$<220$	$>1.8$	
B SMMJ 16403+46437		$5.8 \pm 1.7$	$-2 \pm 8$	593	0.8	
C SMMJ 16404+4643		$<5.7$	$26 \pm 8$	$280/9100$	$0.9(0.2)$	
D SMMJ 16404+4644		$6.3 \pm 2.0$	n/a <sup>f</sup>	1270	0.4	
Abell 2261						
A SMMJ 17223+3207 <sup>g</sup>		$17.6 \pm 3.9$	$-56 \pm 105$	$<452$	$>1.6$	

<sup>a</sup> Positional errors for SCUBA sources with identifications at radio and optical wavelengths (e.g. Ivison et al. 1998b, Frayer et al. 1999) are  $\sim 6$  arcsec for  $4\sigma$  detections and  $\sim 8$  arcsec for  $3\sigma$  detections.

<sup>b</sup> Estimated flux densities with  $1\sigma$  errors. All non-detection upper limits are given as 95 per cent Bayesian confidence regions, assuming Gaussian errors and neglecting the negative flux region

<sup>c</sup> Bayesian 95 per cent limits at 1.4 GHz for sources in A 520, Zw 3146, MS 1455, A 2219, and A 2261, have been extrapolated from the value at 4.9 GHz, using a spectral index  $\alpha = 0.8$  appropriate for star formation driven synchrotron emission. For the data from Stocke et al. (1999), only  $3\sigma$  upper limits are given.

<sup>d</sup> Redshift estimate using Carilli & Yun (1999) radio/far-IR correlation.

<sup>e</sup> In cases where there is ambiguity between the central cluster galaxy and a background galaxy, the radio flux of the cluster galaxy is also listed, and the cluster redshift is given in brackets.

<sup>f</sup> This source falls at the very edge of the short wavelength array.

<sup>g</sup> These sources were verified with 850/450  $\mu$ m photometry. See text for details.

with a cooling flow or could be associated with the Sunyaev-Zel'dovich effect – in either case the emission would have to be very strong and isolated to a small region of the cluster. For this particular cluster, the in-field chop reveals signs of the negative beams. However, another map of this cluster, observed with a large chop for Sunyaev-Zel'dovich increment measurement (Halpern et al. in preparation) suggests that additional source structure in the central region would significantly distort a clear offbeam signature. The extended nature of this central source (also verified in our independent map) is most likely to be a blend of two or more sources.

For the purposes of Table 2 we treat this as a single source. Positions and flux density estimates for such blends should be treated with some caution until higher resolution images are available.

### Abell 520

A large gradient appears to be present across the field, as evidenced by the increased positive excursions in the lower halves of both the 450 and 850  $\mu$ m images and negative excursions in the upper half. This could either be real or due to some residual atmospheric signal – we could not find a convincing way to tell from our data, although we

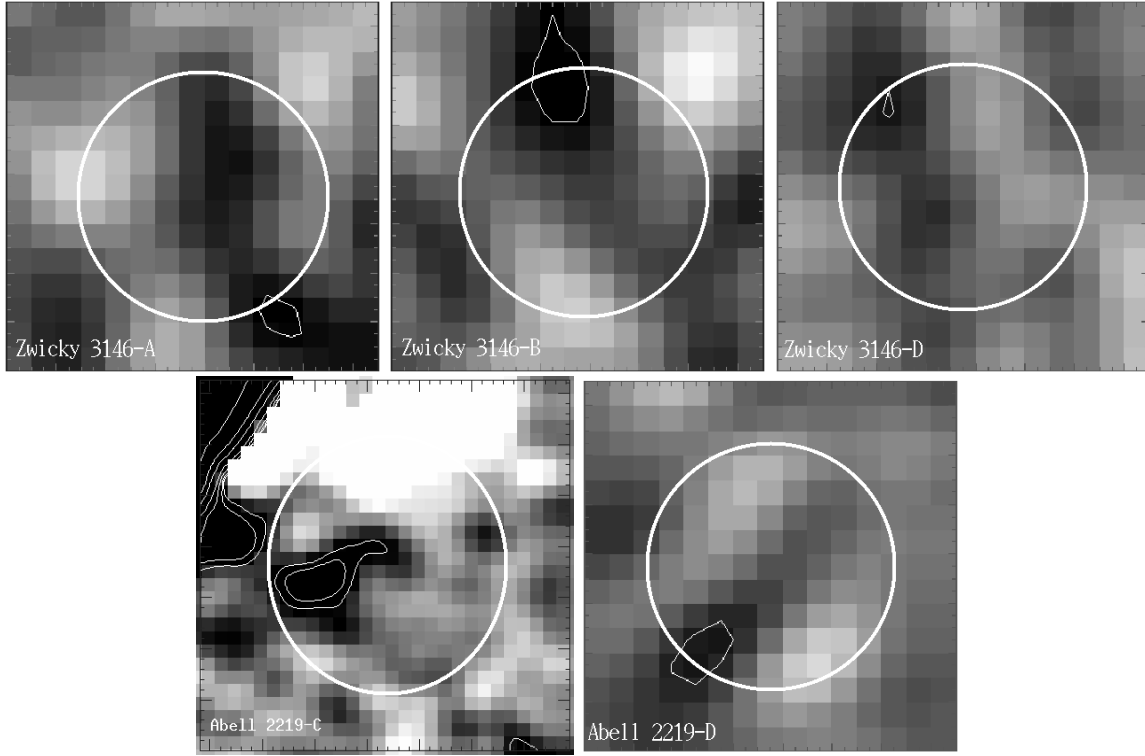


**Figure 3.** VLA counterparts to our sub-mm detected galaxies. We show VLA sources for cases where a  $>3\sigma$  VLA detection is seen relatively nearby the SCUBA position. The radio contours are at 3, 5, 10, 20, 50, 100 and  $200\sigma$  in all cases. The circles are drawn at the positions of sources (see Table 2) from our  $>3\sigma$  SCUBA source catalogue, with 10 arcsec diameter as an estimate of the positional uncertainty. The radio maps are at 4.9 GHz except for Abell 2219-C which is at 1.4 GHz. The other 12 SCUBA sources have only VLA upper limits, as listed in Table 2.

suspect the latter explanation. An apparent  $4\sigma$  source (B: SMMJ 04543+0256) lying to the south of the primary source (A: SMMJ 04543+0257), is  $\sim 3\sigma$  above the noise even once a linear gradient is fit to the plane and subtracted. The flux density presented in Table 2 for this source reflects the subtraction of this linear gradient component. There is no detection of either the BCG or the bright radio source lying to the east in the archive VLA map.

#### Zwicky 3146

The central source in Zw 3146 (A: SMMJ 10237+0411) appears to be extended east-west, and may be another blend. The VLA map reveals that the western extent of the SCUBA source is associated with the BCG, with fairly bright radio emission ( $S_{1.4\text{ GHz}} = 0.92\text{ mJy}$ ). However, the eastern part of the SCUBA source shows no radio emission ( $< 210\text{ }\mu\text{Jy}$ ), and the CY analysis suggests a high redshift background source. Sources B and C in this cluster field also have weak 4.9 GHz detections in the archive VLA map.

#### MS 1054-03

The source in the MS 1054 field (A: SMMJ 10571-0337), has a  $1350/850\text{ }\mu\text{m}$  flux density ratio near unity. As thermal dust emission alone would produce a steep  $\propto \nu^{3.5}$  spectrum, this may indicate that the object has a flat-spectrum AGN radio contribution at  $1350\text{ }\mu\text{m}$ , and perhaps at  $850\text{ }\mu\text{m}$  as well. A bright VLA counterpart, offset by 15 arcsec from the sub-mm peak, has been identified by Condon et al. (1998) as a cluster AGN radio source, and the CY relationship is consistent within errors with the source lying

in the cluster at  $z \sim 0.8$ . However, such a large radio/sub-mm offset is unlikely (see for example Richards et al. 1999), and SMMJ 10571-0337 could easily be a background galaxy lensed by the cluster. Within errors, the  $1350/850\text{ }\mu\text{m}$  ratio is not inconsistent with a higher redshift source. This source has been verified in another SCUBA map of this cluster, although at a slightly lower flux level (P. van der Werf, private communication).

#### MS 1455+22

There is some evidence for  $850\text{ }\mu\text{m}$  SCUBA flux associated with the BCG in the raw MS 1455 maps. However, a somewhat noisy central pixel during the observations of this cluster skews the peak profiles sufficiently that our source finding routine does not identify this as a detection (the source appears at only  $2.6\sigma$  in the final convolved map). We do not include this as a source in our catalogue until it can be verified. However, the proximity of the sub-mm peak to 2 bright radio sources (Fig. 4), and a possible CO(1-0) detection for the BCG (Edge et al. in preparation) lends credence to this putative source. The bright sub-mm source to the south (A: SMMJ 14573+2220) has no VLA counterpart in the archive maps. An additional  $850\text{ }\mu\text{m}$  photometry observation centered on source-A reveals a detection of  $6.8 \pm 1.8\text{ mJy}$ , which is consistent within the relative errors between the mapping and photometry measurements, as well as the extended nature of this source and positional uncertainties.

#### Abell 2163

No sources were found in this cluster field down to a  $3\sigma$

sensitivity of 17 mJy (corresponding roughly to 6 mJy after correction for lensing). This cluster had the poorest sensitivity, and we include it here for completeness only.

#### **Abell 2219**

This map has by far the lowest 450  $\mu\text{m}$  rms, and as a result there are, in addition to the 850  $\mu\text{m}$  detections, two 450  $\mu\text{m}$  detections at the 3 $\sigma$  level. The 1350/850  $\mu\text{m}$  and 450/850  $\mu\text{m}$  ratios and lack of a 4.9 GHz detection for source A (SMMJ 16403+46440) are consistent with the high redshift predicted from CY. This is the only source in A 2219 that does not have at least positive flux density in the VLA archive map. The central source (C: SMMJ 16404+4643), is  $\simeq 2.2\sigma$  at 850  $\mu\text{m}$  but has a fairly clear detection at 450  $\mu\text{m}$ . It does not quite align with the central galaxy radio emission (see Fig. 4), but within errors, it is possible that the source is a cluster member. Indeed the large implied 450/850  $\mu\text{m}$  flux density ratio is indicative of a rather low redshift source. In the archive 1.4 GHz map, however, there is a 5 $\sigma$  source lying near the SCUBA centroid, offset  $\sim 7$  arcsec from the BCG. Source D (SMMJ 16404+4644) lies near the edge of the frame (and off the 450  $\mu\text{m}$  frame entirely), and is only 3 $\sigma$  above the local noise level. However the centroid is within 5 arcsec of an ISO 15  $\mu\text{m}$  source (Barvainis, Antonucci & Helou 1999), with which the sub-mm source may be associated.

#### **Abell 2261**

Although the bright ( $>4\sigma$ ) source to the west (A: SMMJ 17223+3207) does not correspond with any radio emission, the central 2.5 $\sigma$  peak in the SCUBA map is identified with a radio source coincident with the optical BCG (Fig. 4). An additional 850  $\mu\text{m}$  photometry observation centered on source-A reveals a detection of  $13.6 \pm 2.8$  mJy, which is consistent within the relative errors between the mapping and photometry measurements, as well as the extended nature of this source and positional uncertainties.

### **4.3 Cooling flows and centrally concentrated dust emission**

The high central densities of the x-ray gas in many luminous clusters lead to predicted cooling times shorter than the Hubble time (e.g. Fabian 1994). This cooling gas, which can not support the pressure exerted by the overlying hot gas, is expected to flow into the cluster centre. Supporting evidence for such cooling flows is now available in the form of inverted x-ray temperature profiles (e.g. Buote 1999), and x-ray emission lines show gas that has lost most of its thermal energy. The fate of this cool gas remains controversial (e.g. Braine & Dupraz 1994) as no sink has yet been clearly identified.

Observations of the central cluster galaxies in cooling-flow clusters indicate that the cooling flows are not forming large numbers of stars. On the other hand, such stars could be hidden if the initial mass function is biased towards low masses, making the integrated stellar spectrum difficult to detect (e.g. Fabian, Nulsen & Canizares 1982; Mathews & Brighenti 1999). However, the emission-line nebulosity around the central galaxies in many cooling-flow clusters, seen on scales of up to 100 kpc, have emission-line ratios suggestive of large amounts of dust in the central regions – this dust could obscure any stars formed there (Hansen, Jørgensen & Nørgaard-Nielsen 1995; Allen et al. 1995). *HST*

imaging of central cluster galaxies (e.g. for Abell 1795 – McNamara et al. 1996; Pinkney et al. 1996, for Abell 2597 – Koekemoer et al. 1999) has also directly detected dust lanes in some cases. At present the total amount or temperature of this dust is difficult to estimate from the scant observational evidence. Whether the observed dust originate from the cooled gas clouds themselves or from the on-going star formation remains unknown.

SCUBA data may help here by probing emission from cool dust in or around the central galaxies in clusters. The implications of detected cool dust in the BCG of massive clusters for the interpretation of star formation in cooling-flow galaxies, has been discussed in Annis & Jewitt (1993) and Edge et al. (1999). Although there are no highly significant detections of the BCGs in our sample, 3 of the clusters show a marginal positive flux density at 850  $\mu\text{m}$  ( $\sim 2.5\sigma$ ) near the BCG. In Abell 2219, a 3.5 $\sigma$  detection at 450  $\mu\text{m}$  (2.3 $\sigma$  at 850  $\mu\text{m}$ ) lies very near a radio luminous BCG (Fig. 4). In addition, the cluster MS 0451 shows an extended 4 $\sigma$  detection near the x-ray centroid (Donahue 1996), although the brightest cluster galaxy is offset from this position by 23 arcsec, and the only radio source in the vicinity is offset to the other side by 20 arcsecs. Radio maps of the 4 cluster centres with possible BCG detection, along with 10 arcsec sub-mm error circles for reference, are shown in Fig. 4.

Molecular gas, traced by CO emission, might also be present in strong cooling flows (Braine et al. 1995). For MS 1455, we also obtained an upper limit on the CO(4-3) emission from the BCG, which suggests a gas-to-dust ratio of  $\lesssim 150$  if the SCUBA peak were actually a detection. This would be somewhat unusual for known properties of dusty BCGs (Edge et al. 1999), but a weak CO(1-0) detection for the MS 1455 BCG (A. Edge, private communication) lends support to a possible SCUBA detection.

If the SCUBA detection in MS 0451 is associated with a cooling flow, then it is fairly unusual, and may indicate a massive, but highly obscured optical counterpart is actually being built by cooling flow fallout at the true centre of the cluster potential.

We can place limits on the dust mass for the BCG for all clusters in our sample, by considering the 850  $\mu\text{m}$  flux density limit at the redshift of the BCG (see Edge et al. 1999), and adopting model dust parameters, for example  $T_d = 40$  K, with an emissivity index of 1.5. These limits along with the position of the BCG are presented in Table 3. Corresponding CO(1-0) detections and limits, as well as broader implications for cooling flows are presented in Edge et al. (in preparation). The limits are generally much less than the total mass deposition implied by the cluster cooling flows. But our observations are restricted to emission around the BCG, and in any case the limits are model dependent. Any conclusions we draw must necessarily not be very strong. Our non-detections or relatively weak sub-mm emission from most BCGs in a sample of nine clusters, imply that substantial effort will be required to detect other central cluster galaxies. And that if some of the mass is being deposited as cool dust, this will be hard to detect in typical central cluster galaxies with current instrumentation.

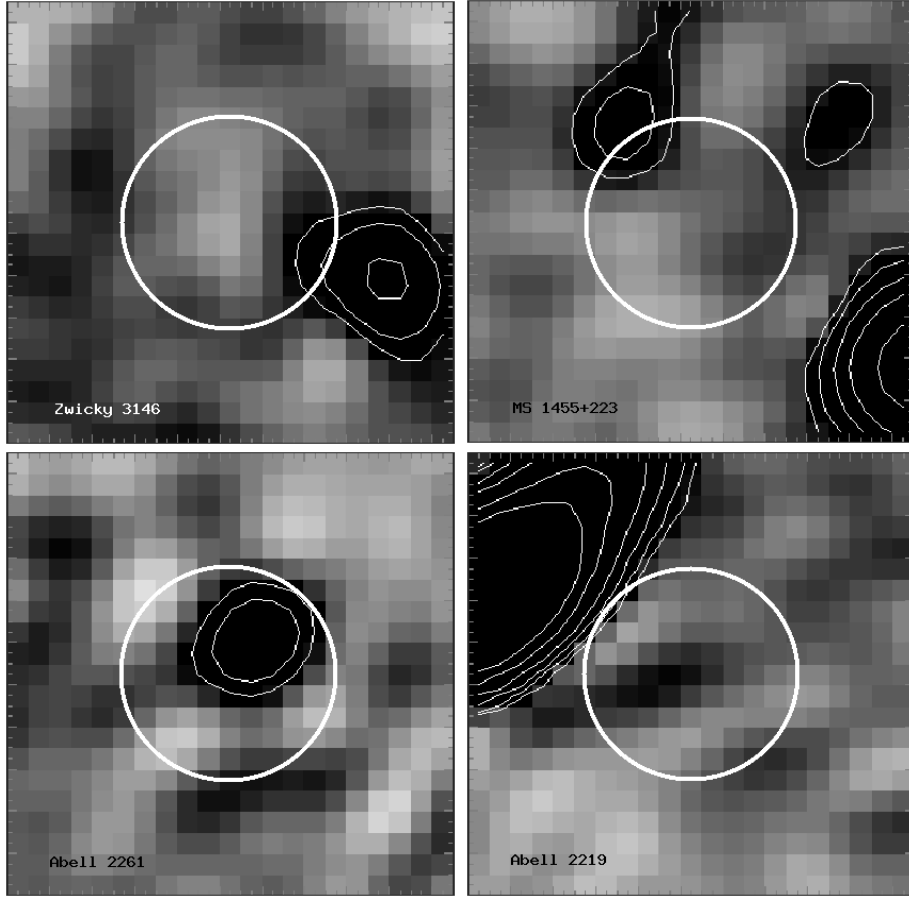


**Figure 4.** VLA 4.9 GHz maps surrounding the brightest cluster galaxies in Zw 3146, MS 1455, A 2261, and A 2219. The field size is  $21 \times 21$  arcsecs in all cases. Radio contours are 3, 5, 10, 20, 50 and 100 times the RMS of the VLA map region. A 10 arcsec diameter error circle is overlaid to indicate the SCUBA beam position, for these marginal  $2-3\sigma$  850  $\mu$ m detections.

Table 3  
Limits on dust mass for central cooling flows.

Cluster	R.A. <sup>a</sup> (J2000)	Dec. <sup>a</sup> (J2000)	$S_{850}^b$ (mJy)	$S_{450}^b$ (mJy)	Dust mass <sup>c</sup> $h_{50}^{-2} M_{\odot}$	$M_{\odot}/\text{yr}^d$
CL 0016+16	00 18 33.2	+16 26 18	< 6.1	< 66	< $4.2 \times 10^8$	n/a
MS 0451-03	04 54 13.4	-03 01 47	$19.1 \pm 4.2$	< 354	$1.3 \times 10^9$	n/a
Abell 520	04 54 19.0	+02 56 49	< 10.0	< 116	< $2.5 \times 10^8$	< 85
Zwicky 3146	10 23 39.6	+04 11 10	$6.6 \pm 2.6$	< 48	$2.4 \times 10^8$	1358
MS 1054-03	10 56 06.2	-03 37 27	< 8.4	< 203	< $8.5 \times 10^8$	n/a
MS 1455+22	14 57 15.1	+22 20 35	$5.3 \pm 2.1$	< 42	$1.5 \times 10^8$	1227
Abell 2163	16 15 34.1	-06 07 26	< 11.3	< 86	< $3.1 \times 10^8$	< 90
Abell 2219	16 40 20.5	+46 42 59	$3.6 \pm 1.7$	$26 \pm 8$	$9.0 \times 10^7$	< 485
Abell 2261	17 22 24.1	+32 07 45	$9.5 \pm 3.8$	< 205	$1.8 \times 10^8$	680

<sup>a</sup> BCG position.

<sup>b</sup> Where no positive value  $> 2.0\sigma$  is detected, we quote Bayesian 95 per cent upper limits.

<sup>c</sup> Assuming  $T_d = 40$  K and  $\beta = 1.5$ , with  $h_{50} = H_0/100 \text{ km s}^{-1} \text{Mpc}^{-1}$ .

<sup>d</sup> Mass deposition values from Allen (2000). The three high- $z$  clusters do not have the x-ray spatial resolution for accurate deprojection (Donahue et al. 1999)

## 5 SOURCE COUNTS

Source count models for rich cluster fields in the sub-mm have been studied in detail by Blain (1997) and Blain et al. (1999), with observational constraints presented in Smail et al. (1997) and Ivison et al. (2000). For unmagnified blank fields, the sub-mm galaxy counts can be derived by simply

dividing the number of detected sources by the surveyed area, although the effects of clustering may have to be considered in small fields (Scott & White 1999). The situation is more complicated in the case of lensing due to a massive cluster, since the source plane is both distorted and magnified at a level dictated by the source redshift and position.

Thus in the image plane, various regions are observed to different depths. Although our clusters were not chosen to provide the largest lensing amplification, the models of Blain (1997, figure 4) show that our cluster redshifts are essentially optimal for maximum amplification, with the exception of MS 1054 which has slightly too high a redshift, but still incurs a reasonably large lensing amplification.

We model the amplification for each source and the effective depth of the source plane area observed using an elliptical potential model of each cluster (Kormann et al. 1994, Newbury 1997). Parameters for the models are derived from both our own imaging data and from the best current information available in the literature. The lensing inversion is based on the prescription of Kormann et al. (1994) and Newbury & Fahlman (1999), allowing a calculation of the lensing amplification and distortion as a function of position in the image plane. Table 4 presents the parameters for each cluster along with an estimate for the lensing amplification at each source position. Columns list the cluster name, redshift, cluster velocity dispersion, angular distance and position angle from North of each source relative to the x-ray centroid, and resulting lens amplification. The final column lists the reference for the cluster parameters. All distances assume a flat  $\Lambda$ -dominated cosmology with  $\Omega_M = 0.3$ .

The essential parameters of the model are the redshift of the cluster and the 1-D (line-of-sight) velocity dispersion ( $\sigma_V$ ), the latter being essential for setting the mass scale. These two quantities set the length scale in the image plane. Larger cluster redshifts reduce the effective magnification, while larger cluster velocity dispersions (cluster mass) increase the magnification. Although more detailed mass models can in principle be constructed using the radial velocities of the individual cluster members (see Blain et al. 1999a), the errors in the source counts are of order 30 per cent, and our results would be very little affected by the use of such cluster mass models.

There is still an ambiguity associated with the unknown background source redshift. However, the models can be used to constrain the range of possible magnifications. For sources at reasonably large redshift ( $z > 1$  say), we find that the cumulative source counts depend fairly weakly on the actual source redshift (less than 30 per cent scatter) in agreement with Blain et al. (1999a). If all sources are assumed to lie at  $z > 2$ , the scatter reduces further. We assume for simplicity that all sources lie at  $z = 2$ . Based on our CY radio analysis of the source redshifts, this is a reasonable assumption, although some sources may in fact lie at somewhat lower redshifts, especially if their dust temperatures are colder than 50 K.

The cluster ellipticity ( $E$ ) is chosen based on an outer contour for the central galaxy, if one exists. In the absence of this BCG contour, we assume circular symmetry. The ellipticity is important only in the case of sources near the cluster centre such as in Zw 3146. The core radius ( $R_{\text{core}}$ ) of the cluster is a model-dependent parameter – the core radius of the x-ray gas being temperature dependent. However for clusters with lensed arcs in their image, it is possible to estimate the core radius directly. Again, the magnification is particularly sensitive to this number only near the cluster centre, as it sets the location of the critical lines with very large magnification. The ellipticity and core radius are quasi-independent parameters of the models. For modest values of

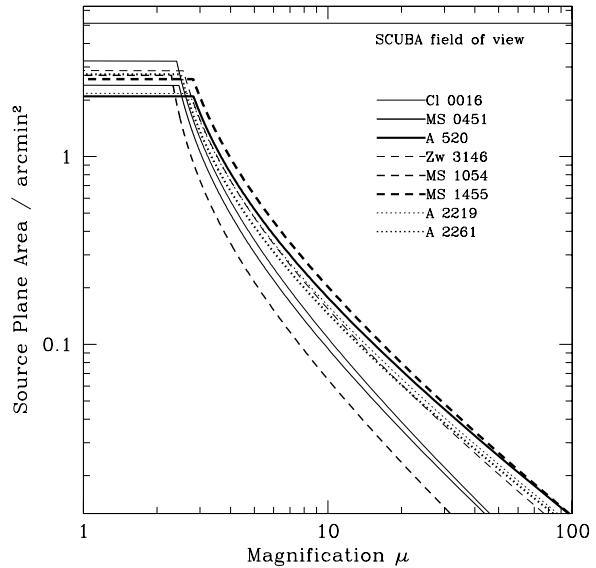


**Figure 5.** Amplification vs area in the source plane for the 8 clusters in our sample with detected sources.

the ellipticity, this parameter plays a very small role, especially in view of all the other uncertainties involved.

Lensing increases the brightness of sources and also magnifies the area – so we reach to fainter effective flux limits, but over a smaller effective solid angle. Fig. 5 shows the resulting magnification vs source plane area for each cluster. Our complete survey area in the source plane is in fact only  $\sim 19 \text{ arcmin}^2$ , from a total surveyed SCUBA field area of  $\sim 47 \text{ arcmin}^2$ . We estimate that the uncertainties in cluster parameters ( $\sigma_V$ ,  $R_{\text{core}}$ ,  $E$ ) to the lensing model contribute  $\sim 25$  per cent error, a little larger than the errors in calibrating SCUBA maps, but less than the Poisson error in the source counts themselves.

## 6 RESULTS

With the lensing factored in, our effective noise level in the central regions of the cluster fields decreases sharply, as displayed in Fig. 6. From these relations of sensitivity as a function of cluster area, we can calculate the effective area surveyed to a given depth. Fig. 7 shows the integral source counts from our survey including all sources detected at  $> 3\sigma$  (solid circles, binned). We plot the counts from the Smail, Ivison, Blain (1997) lensing survey presented in Blain et al. (1999c, crosses), as well as a fit to the combined blank field sub-mm counts (Hughes et al. 1998, Barger et al. 1999b, Eales et al. 1999) constrained at faint fluxes to not overproduce the far-IR background (dotted line). When we restrict ourselves to the  $> 4\sigma$  sub-set which contains no obvious cluster members there is no dramatic change in the counts (open circles in Fig. 7). We fit these  $4\sigma$  counts with a simple power law  $N(>S) = N_0(S/S_0)^{-\gamma}$ , with  $S_0 = 1 \text{ mJy}$ , and find  $\gamma \simeq 1.73$ , and  $N_0 \simeq 11200$ . These are close to the blank field values of  $\gamma = 2.2$ , and  $N_0 = 13600$ . A direct comparison with other published sub-mm source counts thus reveals a

Table 4  
Lensing parameters for clusters

Cluster	$z$	$\sigma_V$ (km s $^{-1}$ )	$\Delta\theta_{\text{source}}$ (PA) <sup>a</sup>	Lens amplification	Cluster reference
Cl 0016+16	0.541	1243	44(138), 62(171)	3.0, 2.6	Ellingson et al. 1998
MS 0451-03	0.550	1353	65(130), 25(46)	2.6, 4.5	Donahue (1996)
Abell 520	0.203	927	61(104), 74(138)	3.4, 3.1	Gioia & Luppino (1994)
Zwicky 3146	0.291	1310	31(117), 62(179), 69(-33), 78(-136)	6.8, 3.7, 3.5, 3.2	Ebeling et al. (1996)
MS 1054-03	0.833	1170	63(70)	2.6	Donahue et al. (1998)
MS 1455+22	0.259	1168	58(162.5)	2.8	Stocke et al. (1991)
Abell 2163	0.201	1231	n/a	n/a	Gioia & Luppino (1994)
Abell 2219	0.228	1000	66(17), 45(157), 15(178), 41(-93)	3.6, 3.2, 7.5, 3.0	Smail et al. (1996)
Abell 2261	0.224	1102	72(-124)	3.3	Ebeling et al. (1996)

<sup>a</sup> Distance and position angle of the sources (listed in Table 2) from the x-ray centre.

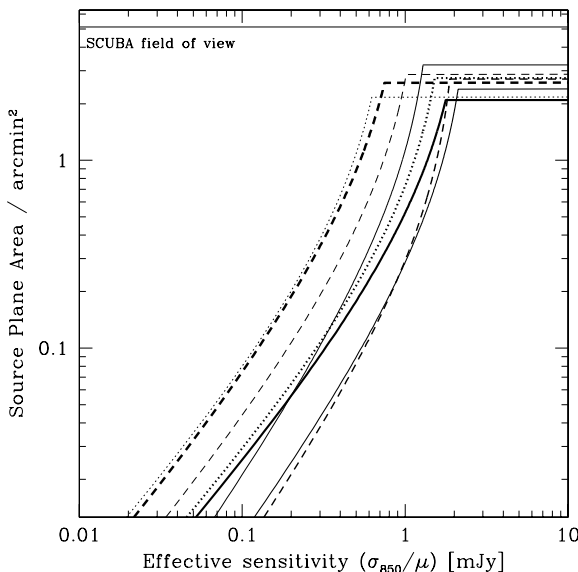


Figure 6. Area vs sensitivity for the 8 clusters in our sample with detected sources. Line types are the same as in Fig. 5.

good agreement between results, including gravitationally lensed and blank field counts. SCUBA preferentially selects galaxies with  $z \gtrsim 1$ , due to the spectral shape at these wavelengths. Therefore we expect few detections in the clusters themselves, however, this may be the source of some of the small discrepancy between the various surveys.

A positive magnification from the cluster lensing means that we are seeing fainter galaxies, and hence an increase in the surface density of galaxies. However, this is offset by the loss in area due to field distortion. If the source count power-law index were too shallow, this would result in a less efficient survey compared to a blank field survey with equivalent integration time. However, our results show a net positive bias, so that we are detecting more sources per unit time and at unlensed flux densities below what would be possible in blank field searches, in line with what was found earlier by Smail et al. (1997).

Using the amplification due to the foreground cluster, lensed surveys also suffer less from confusion noise (e.g. Blain et al. 1998). The large beamsize of SCUBA implies a con-

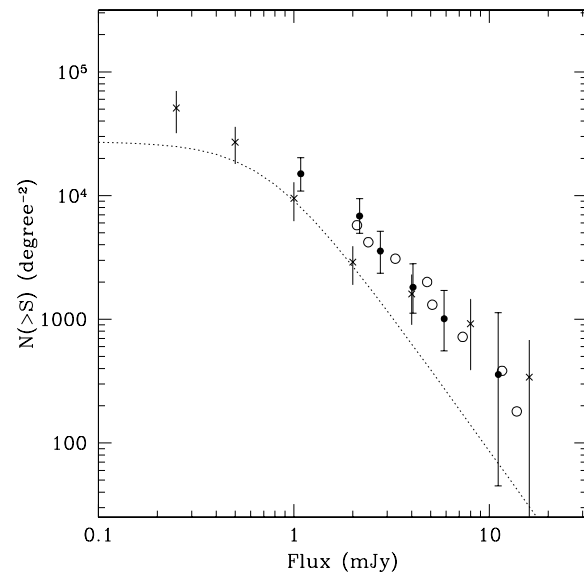


Figure 7. The integral source counts (number of objects brighter than flux density  $S$  as a function of  $S$ ). We plot our total counts of  $> 3\sigma$  detections (solid circles, binned), and our sub-sample excluding possible cluster members and detections less than  $4\sigma$  significance (open circles, individual sources). The corrected counts from Blain et al. (1999c) are plotted with crosses. The dotted line depicts a fit to the combined blank field sub-mm counts (Hughes et al. 1998, Barger et al. 1999b, Eales et al. 1999) constrained at faint fluxes to not overproduce the far-IR background. The error bars shown for our complete sample points are  $\pm 1\sigma$  (68 per cent Bayesian confidence region) errors based on Poisson statistics.

fusion limit at  $\sim 1.5$  mJy, while we have detected 4 possible sources fainter than 2 mJy.

## 7 DISCUSSION

Estimates of the redshift distribution for the SCUBA-selected sources remain in dispute (Hughes et al. 1998; Barger et al. 1999a; Lilly et al. 1999a). Hughes et al. (1998) concluded that the bulk of the population is at  $z \sim 2-4$ , based on photometric redshift limits for the probable counterparts of five sub-mm sources in the Hubble Deep Field (c.f. Richards 1999; Downes et al. 1999). Barger et

al. (1999a) undertook a spectroscopic survey of the Smail et al. (1999) sub-mm sample and concluded that the median redshift was  $\sim 1.5$ –2, with the bulk of the population having  $z \sim 1$ –3. Lilly et al. (1999a) used archival spectroscopy and broad-band photometry of sub-mm sources from the Eales et al. (1999) survey to conclude that the population spans  $z = 0.1$ –3, with a third at  $z < 1$ . Given the relatively small number statistics and the very real possibility of some misidentifications, it is unclear whether there is any genuine disagreement.

However, use of the Carilli & Yun (CY – 2000) relation of radio/far-IR flux to predict the redshifts for a large sample of SCUBA sources (Smail et al. 2000), has suggested that the population may have a median value lying between  $z = 2.5$  and 3. This is consistent with our CY analysis using VLA maps, which result in a median value lying at  $z \gtrsim 2.0$ , although dependent on the dust temperature and emissivity adopted. Fig. 8 shows an estimate of the cumulative redshift distribution for our entire sample, derived from the CY relation using radio detections and lower limits. Also depicted are the cumulative redshift distributions for models formulated to fit the far-IR background, and various infrared counts, by Guiderdoni et al. (1998), and Blain et al. (1999b).

The archival radio maps for many of our cluster fields are not deep enough to put strong constraints on the redshift distribution of sub-mm sources, with few actual radio detections. Given that the derived redshifts are generally lower limits, it is difficult to presently discriminate between predictions for the redshift distribution from various models (e.g. Blain et al. (1999b) model Gaussian and modified Gaussian models (long and short dashes) or the Guiderdoni et al. (1998) model (dotted line)). However, the radio/far-IR correlation indicates that the bulk of the dust emission in the universe did not occur at redshifts much below  $z = 2$ . The true redshift distribution remains to be determined. Deep optical and near-IR imaging should also uncover these objects' optical properties, and resolve currently unanswered questions such as whether the galaxies would be detectable through their Lyman break (Chapman et al. 2000), or whether they have extremely red colours (Smail et al. 1999).

We can calculate lower limits to the far-IR background radiation intensities from measured flux densities of resolved  $4\sigma$  sources in our cluster fields. The contribution is the sum  $\Sigma(S/A)$ , where  $A$  is the area which has a sensitivity necessary to see a source of flux  $S$ , where lensing has been factored into the sum. We find  $9.1 \text{ Jy deg}^{-2}$  averaged over all 9 fields. This corresponds to 20 per cent of the total FIRB at  $850 \mu\text{m}$  as measured by Fixsen et al. (1998):  $44 \text{ Jy deg}^{-2}$ . The accuracy of these estimates however depends on the lensing models and other details of the counts, together with the remaining uncertainty in the FIRB measurement at these wavelengths. If we take the simple power law model integrated up from 1 mJy, then the background is  $N_0\gamma/(\gamma - 1)$ . Using our slope from Fig. 7 accounts for more than half of the background down to 1 mJy.

## 8 CONCLUSIONS

(i) We have detected 17 new sub-mm sources in the fields of 9 rich galaxy clusters. Comparison with VLA radio images

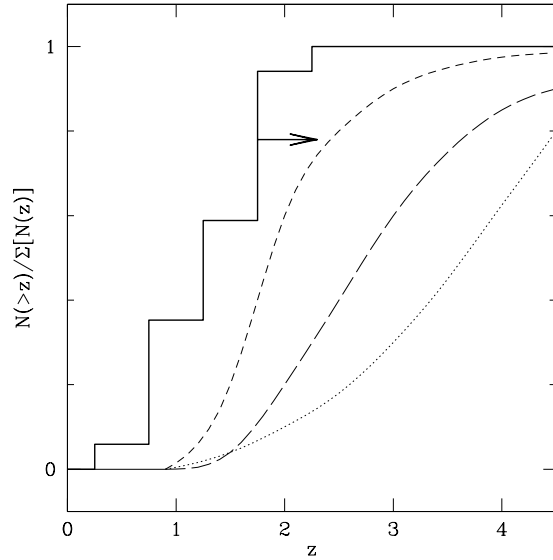


**Figure 8.** Cumulative redshift distribution estimated for our entire sample, derived from the CY relation using VLA data (solid line). Also shown are the cumulative redshift distributions for models formulated to fit the far-IR background, and various infrared counts, by Guiderdoni et al. (1998) – dotted line, Blain et al. (1999b) Gaussian model of luminosity evolution – long-dashed line, and Blain et al. (1999b) modified Gaussian model fit to the Barger et al. (1999a) redshift distribution – short-dashed line.

suggests that most of these are being lensed by the cluster mass, rather than being in the clusters themselves.

(ii) We see no strong evidence for cool dust emission around BCGs, which might be related to cooling flows.

(iii) Our sub-mm source counts are in reasonable agreement with existing sub-mm surveys, and extend the list of such sources available for follow up at other wavelengths.

(iv) The redshift distribution has been loosely constrained using the radio-far-IR correlation, and favours a relatively high redshift ( $z > 2$ ) for the bulk of dust emission in the Universe.

## ACKNOWLEDGEMENTS

This work was supported by the Natural Sciences and Engineering Research Council of Canada. The James Clerk Maxwell Telescope is operated by The Joint Astronomy Centre on behalf of the Particle Physics and Astronomy Research Council of the United Kingdom, the Netherlands Organisation for Scientific Research, and the National Research Council of Canada. We would like to acknowledge the staff at JCMT for facilitating these observations. The VLA is run by NRAO and is operated by Associated Universities Inc., under a cooperative agreement with the National Science Foundation.

## REFERENCES

Allen S.W., Fabian A.C., Edge A.C., Böhringer H., White D.A., 1995, MNRAS, 275, 741

Allen S.W., 2000, MNRAS, 315, 269

Andreani P., Bohringer H., dall'Oglio G., Martinis L., Shaver P., et al., 1999, ApJ, 513, 23

Annis J., Jewitt D., 1993, MNRAS, 264, 593

Barger A.J., Cowie L.L., Sanders D.B., Fulton E., Taniguchi Y., et al., 1998, Nature, 394, 248

Barger A.J., Cowie L.L., Smail I., Ivison R.J., Blain A.W. et al., 1999a, AJ, 117, 2656

Barger A.J., Cowie L.L., Sanders D.B., ApJ, 518 L5

Barvainis R., Antonucci R., Helou, G., 1999, AJ, 118, 645

Bertoldi F., Carilli C.L., Menten K.M., Owen F., Dey A., et al., 2000, submitted to A&A [astro-ph/0006094]

Birkinshaw, M., 1999, Phys. Rep., 310, 97

Blain A.W. 1997, MNRAS, 290, 553

Blain A.W., Ivison R.J., Smail I. 1998, MNRAS, 296, L29

Blain A.W., Smail I., Ivison R.J., Kneib J.-P. 1999a, ApJ, 512, L87

Blain A.W., Smail I., Ivison R.J., Kneib J.-P. 1999b, MNRAS, 302, 632

Blain A.W., Ivison R.J., Kneib J.-P., Smail I., 1999c, in 'The High Redshift Universe: galaxy formation and evolution at high redshift', eds. A.J. Bunker & W.J.M. van Breughel, ASP conference vol193 ASP: San Francisco, p.246-249

Blain A.W., 1999, MNRAS, 309, 955

Borys C., Chapman S.C., Scott D., 1999, MNRAS, 308, 527

Braine J., Dupraz C. 1994, A&A, 283, 407

Braine J., Wyrowski F., Radford S.J.E., Henkel C., Lesch, H., 1995 A&A, 293, 315

Buote D.A., 1999, MNRAS, 309, 685

Carilli C.L., Yun M.S., 1999, ApJ, 513, L13

Carilli C.L., Yun M.S., 2000, ApJ, 530, 618

Carlstrom J., Joy M., Grego L., Holder G., Holzapfel W., et al., 1999, 'Particle Physics and the Universe', Physica Scripta and World Scientific, eds. L. Bergstrom, P. Carlson and C. Fransson, [astro-ph/9905255]

Chapman S.C., Scott D., Lewis, G., Borys C., Fahlman G.G., 1999, A&A, 352, 406

Chapman S.C., Scott D., Steidel C., Borys C., Halpern M., Morris S., Adelberger K., Dickinson M., Giavalisco M., Pettini M., 2000a, MNRAS, in press [astro-ph/9909092]

Crawford C., Allen S., Ebeling H., Edge A., Fabian A., 1999, MNRAS, 307, 91

Donahue M., 1996, ApJ, 468, 79

Donahue M., Voit M., Gioia I., Luppino G., Hughes J., Stocke J., 1998, ApJ, 502, 550

Donahue M., et al., 1999, ApJ, 527, 525

Downes D., Neri R., Greve A., Guilloteau S., Casoli F., et al., 1999, A&A, 347, 809

Eales S.A., Lilly S.J., Gear W.K., Bond J.R., Dunne L., et al., 1999, ApJ, 518, L641

Ebeling H., Voges W., Böhringer H., Edge A., Huchra J., et al., 1996, MNRAS, 281, 799

Edge A.C., Ivison R.J., Smail I., Blain A.W., Kneib J.-P., 1999a, MNRAS, 306, 599

Ellingson E., Yee H.K., Abraham R.G., Morris S.L., Carlberg R., 1998, ApJS, 116, 247

Fabian A.C., 1994, ARAA, 32, 277

Fabian A.C., Nulsen P.E.J., Canizares C.R., 1982, MNRAS, 201, 933

Fixsen D.J., Dwek E., Mather J.C., Bennett C.L., Shafer R.A., 1998, ApJ, 508, 123

Frayer D., Smail I., Ivison R.J., Scoville N.Z., 2000, ApJ, in press

Frayer D., Ivison R.J., Scoville N.Z., Evans A.S., Yun M., et al., 1999, ApJ, 514, L13

Frayer D., Smail I., Ivison R.J., Scoville N.Z., Yun M., Evans A.S., et al., 1998, ApJ, 506, L7

Gear W., Lilly S., Stevens J., Clements D., Webb T., Eales S., Dunne L., 2000, MNRAS, in press, astroph/0007054

Gioia I.M., Luppino G.A., 1994, ApJS, 94, 583

Guiderdoni B., Bouchet F.R., Puget J.-L., Lagache G., Hivon E., 1997, Nature, 390, 257

Guiderdoni B., Hivon E., Bouchet F.R., Maffei B., 1998, MNRAS, 295, 877

Hansen L., Jorgensen H.E., Norgaard-Nielsen H.U., 1995, A&A, 297, 13

Hauser M.G., Arendt R.G., Kelsall T., Dwek E., Odegard N., et al., 1998, ApJ, 508, 25

Holland W.S., Robson E.I., Gear W.K., Cunningham C.R., Lightfoot J., et al., 1999, MNRAS, 303, 659

Hughes D.H. et al. 1998, Nature, 394, 241

Ivison R.J., Dunlop J.D., Hughes D.H., Archibald E., Stevens J.A., et al., 1998a, ApJ, 494, 211

Ivison R.J., Smail I., Le Borgne J.-F., Blain A.W., Kneib J.-P., et al., 1998b, MNRAS, 298, 583

Ivison R.J., Smail I., Barger A.J., Kneib J.-P., Blain A.S., et al., 2000, MNRAS, in press [astro-ph/9911069]

Jenness T., Lightfoot J.F., Holland W.S., 1998, SPIE, 3357 548 [astro-ph/9809120]

Koekemoer A.M., O'Dea C.P., Sarazin C.L., McNamara, B.R., Donahue, M., et al., 1999, ApJ, 525, 621

Kormann P., Schneider P., Bartelmann M., 1994, A&A, 284, 285

Lilly S.J., Eales S.A., Gear W.K., Hammer F., Le Fèvre O., et al., 1999a, ApJ, 343, 123

Lilly S.J., Eales S.A., Gear W.K., Webb T.M., Bond J.R., et al., 1999b, 'Formation of Galactic Bulges', ed. C.M. Carollo, H.C. Ferguson & R.F.G. Wyse, Cambridge University Press, Cambridge p. 119 [astro-ph/9903157]

Lagache G., Abergel A., Boulanger F., Desert F.X., Puget J.-L., 1999, A&A, 344, 322

Mathews W.G., Brighenti, F., 1999, ApJ, 526, 114

McNamara B.R., Wise M., Sarazin C.L., Jannuzi B.T., Elston, R., 1996, ApJ, 466, L9

Newbury P., 1997, PhD thesis, University of British Columbia

Newbury P., Fahlman, G.G., 1999, preprint [astro-ph/9905254]

Pinkney J., Holtzman J., Garasi C., Watson A.M., Gallagher J.S., et al., 1996, ApJ, 468, L13

Richards E.A., Fomalont E.B., Kellermann K. 1999, ApJ, 526, L71

Richards E.A., 1999, ApJ, 513, L9

Richards E., Kellermann K.I., Fomalont E.B., Windhorst R.A., Partridge R.B., 1998, AJ, 116, 1039

Sanders D.B., 1999, 'Space Infrared Telescopes and Related Science', 32nd COSPAR workshop, ed. T. Matsumoto, T. de Graauw [astro-ph/9904292]

Sanders D.B., Mirabel I.F., 1996, ARAA, 34, 749

Scott D., and White M., 1999, A&A, 346, 1

Smail I., Dressler A., Kneib J.-P., Ellis R.S., Couch W., 1996, ApJ, 469, 508

Smail I., Ivison R.J., Blain A.W. 1997, ApJ, 490, L5

Smail I., Ivison R.J., Blain A.W., Kneib J.-P. 1998, ApJ, 507, L21

Smail I., Ivison R.J., Kneib J.-P., Cowie L.L., Blain A.W., et al., 1999, MNRAS, 308, 1061

Smail I., Ivison R.J., Owen F.N., Blain A.W., Kneib J.-P., 2000, ApJ, 528, 612

Stocke J.T., Morris S.L., Gioia I.M., Maccacaro T., Schild R., et al., 1991, ApJS, 76, 813

Stocke J.T., Perlman E.S., Gioia I.M., Harvanek M. 1999, AJ, 117, 1967